Applied Ocean Research 138 (2023) 103671

Contents lists available at ScienceDirect

Applied Ocean Research

journal homepage: www.elsevier.com/locate/apor

Whole-life modelling of anchor capacity for floating systems: The RSN—CSI approach

K.A. Kwa [a,*], D.J. White [a], T. Tosdevin [b], S. Jin [c], D. Greaves [b]

[a] University of Southampton, Southampton SO17 1BJ, UK
[b] University of Plymouth, Plymouth PL4 8AA, UK
[c] Ocean Institute, Northwestern Polytechnical University, Taicang 215400, China

ARTICLE INFO

Keywords:
Offshore geotechnics
Anchors and foundations
Floating offshore renewable energy
Whole-life geotechnics

ABSTRACT

Successive episodes of cyclic loading cause the strength of soft soils to reduce, through pore pressure build-up, and then recover, through consolidation, as shown by model testing, field studies and theoretical considerations. These 'whole-life' changes in soil strength affect the capacity of anchoring systems for offshore infrastructure such as floating turbines or platforms. This paper introduces a new macro-model for assessing the through-life changes in seabed strength and anchor capacity as a result of variable cyclic loading and concurrent consolidation. The model combines SN curves for damage accumulation with a critical state soil mechanics framework for changes in soil strength and anchor capacity. These methods allow the full operational lifetime of an anchoring system to be rapidly analysed, encompassing timescales from individual wave-induced load cycles, through to annual seasons and soil consolidation processes. The approach provides a new basis for whole-life modelling of anchoring systems that is sufficiently fast to allow reliability-based assessments via a Monte Carlo method. In soft soils that exhibit beneficial gains in capacity, this method provides a basis for more efficient design through reductions in anchor size.

1. Introduction

Offshore infrastructure for renewable energy, oil and gas production is subjected to a wide range of actions from metocean and operational conditions. These actions are transmitted via structures or mooring lines to the foundation or anchoring systems. Over the 'whole-life' or operational lifetime of the infrastructure, these loads can alter the geotechnical properties of the seabed and the capacity and response of the infrastructure. Whole-life geotechnical design couples the life cycle of imposed actions with the evolving geotechnical resistance to forecast the evolving response and reliability of the system across the design life of the infrastructure (Gourvenec, 2020).

In soft soils, a key geotechnical mechanism within 'whole-life' analysis is the beneficial consolidation effects that can cause an increase in strength around offshore foundations, which counteracts the more recognised effect of soil strength reduction from cyclic loading, typically captured by SN curves (Andersen et al. 1988; Andersen 2015). Consolidation gains following loading events have been quantified during flow round penetrometer tests (Hodder et al., 2013; O'Loughlin et al., 2017), direct simple shear element tests (Laham et al., 2021; Laham et al., 2023), large scale laboratory tank tests and geotechnical centrifuge tests of pipelines (Smith and White, 2014), sliding foundations (Cocjin et al., 2014, 2017), anchors (Han et al., 2016; Zhou et al., 2020) and pile foundations (Lai et al., 2020; Bayton et al., 2018; Richards et al., 2018, 2020; Abadie et al., 2019; Truong et al., 2019, Guevara et al., 2020, White et al., 2022).

The examples listed above highlight the potential value in any design approach that quantifies 'whole-life' changes in the capacity and stiffness of foundations and anchors. Firstly, this may allow more accurate assessment of system reliability, including changes in the geotechnical reliability through life. Such an advance would parallel developments in structural reliability analysis, where time-dependent changes – usually a reduction in reliability – are recognised and quantified within models (Bai and Jin 2016). Secondly, the transition of offshore engineering to focus on large numbers of uncrewed renewable energy facilities, which have lower environmental impact potential than oil and gas platforms, creates a stronger impetus to understand system reliability (Cerfontaine et al., 2023.) This is because the consequences of an individual failure are smaller, and therefore target reliability values can be larger and therefore more quantifiable.

To explore this type of design approach, this study presents a macro

* Corresponding author.
E-mail address: k.a.kwa@soton.ac.uk (K.A. Kwa).

https://doi.org/10.1016/j.apor.2023.103671
Received 18 March 2023; Received in revised form 28 May 2023; Accepted 13 July 2023
Available online 1 August 2023

SYMBOLS

A_p	cross sectional area of anchor
B	anchor diameter
c_v	coefficient of consolidation
D	damage
F_{max}	maximum peak anchor force for a sea state
F_T	tension force on anchor
H	hardening
H_s	significant wave height
k_{d2}	scaling parameter
k_i	constants controlling rate of damage accumulation
N	number of cycles
N_c	bearing capacity factor
N_{eq}	equivalent number of cycles
P_f	probability of failure
Q_{ult}	anchor capacity
q	rate of change in sensitivity
R	average cyclic stress or average cyclic load ratio
S	cyclic amplitude stress or cyclic amplitude load ratio
S_t	sensitivity
S_{t0}	initial sensitivity
s_u	undrained shear strength
s_{u0}	initial undrained shear strength
s_{uR}	ratio of the maximum gain in undrained strength to the initial undrained strength
$(s_u/\sigma'_{v0})_{NC}$	normally consolidated undrained strength ratio
T_p	peak wave period
t	time
t_{cyc}	duration of cyclic loads
t_c	duration of intervening consolidation stage
u	pore water pressure
α_{H_s}	scale factor in marginal PDF of H_s
β	scaling parameter
β_{H_s}	shape factor in marginal PDF of H_s
γ	rate of change in hardening
γ'	effective soil unit weight
γ_{H_s}	location factor in marginal PDF of H_s
κ^*	swelling index
λ^*	compression index
μ	location factor for conditional PDF of T_p
σ	shape factor for conditional PDF of T_p

'RSN—CSI' model for assessing the whole-life behaviour of an anchoring system in soft clay during the application of variable amplitude cyclic loads throughout an operational life.

The paper first introduces the model components and how they fit together, which is illustrated in Fig. 1, and consists of:

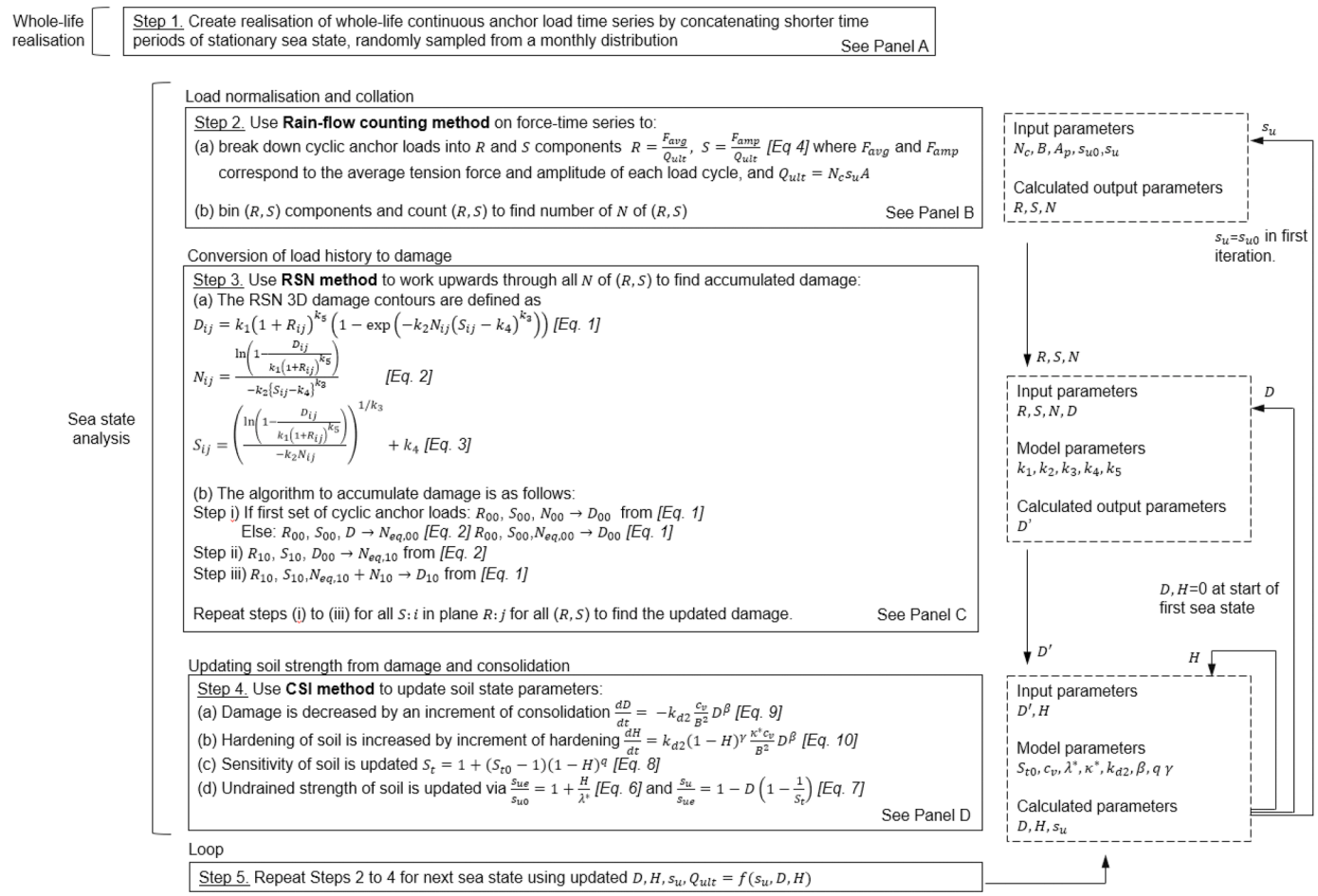

(a)

Fig. 1. (a) Flow-chart and (b) accompanying schematic of embedded plate anchor, anchor loads breakdown and the RSN—CSI model method.

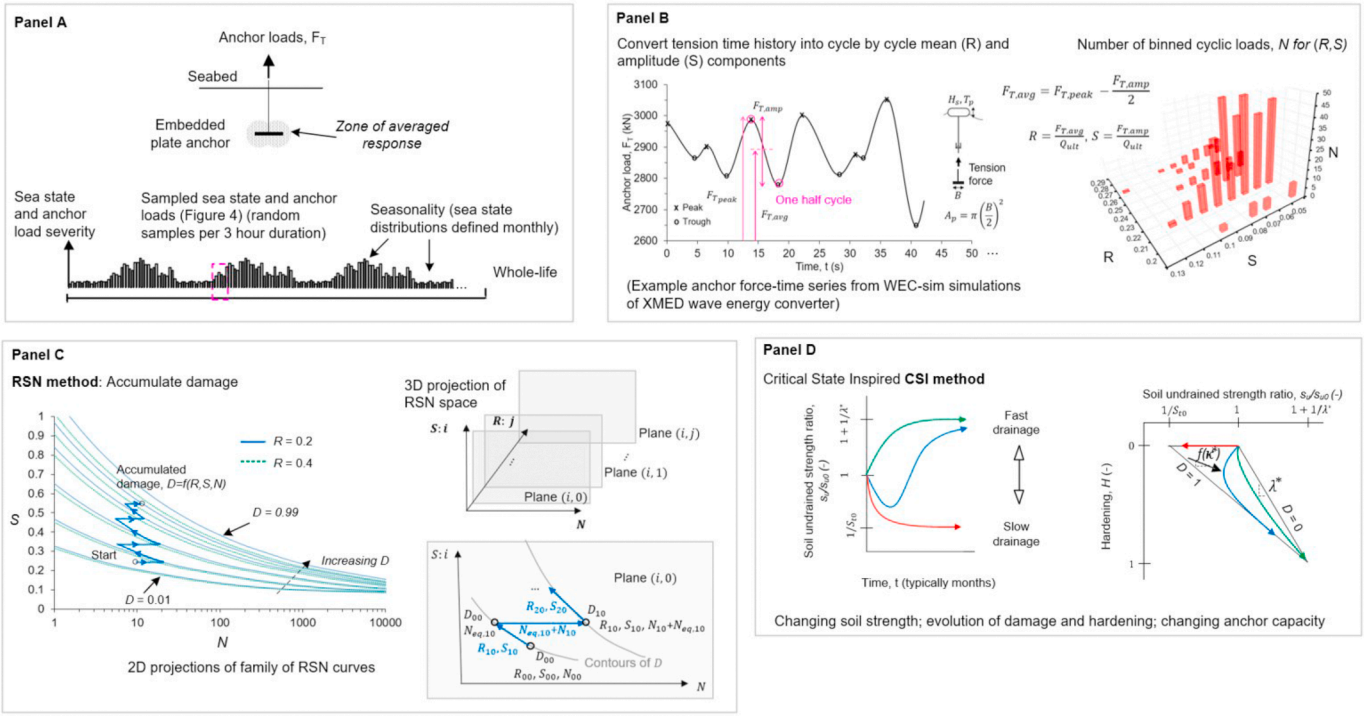

(b)

Fig. 1. (*continued*).

- RSN model: An extended SN model for calculating the accumulation of damage (or reduction in soil strength) from a time series of random cyclic loads, representing a period of stationary weather, (or a 'sea state').
- CSI model: A critical state-inspired model for calculating the combined effects of damage and consolidation on soil strength and anchor capacity, through a sequence of sea states.
- Anchor bearing capacity: A conventional link from soil strength to anchor capacity.

The analysis is firstly illustrated by comparison with two sets of centrifuge model tests with idealised patterns of loading and is shown to give good predictions of the resulting changes in strength and capacity. The approach is then used to simulate the whole-life response of the anchoring system of a taut-moored wave energy converter – the X-MED buoy (Hann et al., 2015). Realistic seasonal weather is considered, based on a location offshore the south-west of the UK, and the changing anchor capacity is simulated. The analysis is expanded using a Monte Carlo approach to investigate the reliability of different sizes of anchor, with and without consideration of whole-life loading effects.

2. RSN model

The purpose of the *RSN* model is to evaluate the scalar parameter, damage, D, that results from a series of random cyclic loads during a sea state. The damage then feeds into the CSI model to quantify the reduction in soil strength caused by the cycles. Damage is analogous to excess pore pressure build-up. Andersen and Lauritzen (1988) and others, quantify damage from a time series of random cyclic loads based on an accumulation approach in which each load cycle is assigned an average cyclic stress ratio value, R and a cyclic amplitude stress ratio value, S, and the number of cycles, N, within binned ranges are combined (Andersen et al., 1988; Andersen, 2009, 2015; Randolph and Gourvenec, 2017).

The *SN* accumulation approach works upwards through the binned cyclic amplitudes converting the accumulated damage at each binned value of S into a number of cycles at the next bin, until the final result is the total damage, D (this result is often expressed as the equivalent number of cycles, N_{eq} at the peak load that would cause the same D). This approach allows the accumulated effect of a general spectrum of loads to be reduced to a single scalar quantity that represents the level of damage experienced by the soil surrounding the anchor.

In this study we use *SN* curves that originate in Verruijt (1995) and were modified in Bonjean et al. (2008) and Tom et al. (2019), to link D, S and N analytically as defined in Eqs. (1 3. These equations have been extended to additionally include the influence of average load and this is captured in the average cyclic stress ratio R term, such that if R=0, Eqs. (1) ((3) reduce back to the original *SN* curve formulation). This extended RSN formulation provides three-dimensional damage contours of similar shape to those shown by Andersen (2015). These *RSN* relationships involve five constants, k_1 to k_5, and can be written with D, S or N as the subject:

$$D = k_1(1+R)^{k_5}\left(1-\exp\left(-k_2 N\{S-k_4\}^{k_3}\right)\right) \tag{1}$$

$$N = \frac{\ln\left(1-\frac{D}{k_1(1+R)^{k_5}}\right)}{-k_2\{S-k_4\}^{k_3}} \tag{2}$$

$$S = \left(\frac{\ln\left(1-\frac{D}{k_1(1+R)^{k_5}}\right)}{-k_2 N}\right)^{1/k_3} + k_4 \tag{3}$$

where $\{\ldots\}$ are Macaulay brackets such that no damage is accumulated when $S < k_4$. The parameter, k_4 therefore sets a minimum cyclic load threshold below which no damage occurs. k_1 represents the maximum possible value of D, which is 1. The parameters k_2, k_3 and k_5 control the rate of damage generation. The selected values of k_1 to k_5 were chosen to provide RSN curves similar to those presented in Andersen (2015) for a normally consolidated soft clay. The *RSN* damage accumulation calculation extends the usual *SN* method by accumulating up each step of R after accumulating in the *SN* plane for each value of R, as illustrated in Fig. 1b Panel C. Also, any damage present at the start of the sea state is

used as an initial value in the accumulation process.

The RSN concept comes from element testing, where R and S are written in terms of stress ratios. In the macro-model concept, foundation loads are linked to the stress mobilised in the surrounding soil via the bearing factor N_c and cross-sectional area of the plate, A_p, in the same way that foundation capacity is linked to soil strength. It is therefore possible to also treat R and S as load ratios, defined accordingly as average cyclic and cyclic amplitude load ratios:

$$R = \frac{F_{avg}}{Q_{ult}},\ S = \frac{F_{amp}}{Q_{ult}} \tag{4}$$

where Q_{ult} is the current ultimate anchor capacity and F_{avg} is defined as

$$F_{avg} = F_{peak} - \frac{F_{amp}}{2} \tag{5}$$

and F_{peak} and F_{amp} correspond to the maximum tension force and amplitude of each load cycle as shown in Fig. 1 Panel B.

The adopted *RSN* model parameters are given in Tables 1 to 3, and were selected based on those presented in Anderson (2015). It is recognised that the shapes of RSN curves for soil element behaviour may not be applicable directly to foundation capacity, although similar scaling has been adopted previously with success (Jardine et al., 2012).

3. CSI model

3.1. Model description

The CSI model is set out by White et al. (2022), and tracks the current soil undrained strength, s_u, which controls the anchor capacity, using two state parameters: damage, D and hardening, H, both of which vary in the range 0 to 1 (see Fig. 1b, Panel D). The model was applied by White et al. (2022) to the capacity and stiffness of a laterally-loaded pile, by integrating the model into a p-y analysis. They used a strain-based approach to damage generation, in which increases in D result from pile movement. That aspect has been replaced in the present study by the *RSN* model for damage generation. This change allows long time series of cyclic loading to be analysed more efficiently, and permits the analysis to use a loading history as input, rather than requiring displacements to be evaluated.

The hardening index H is analogous to voids ratio in critical state terms. Since the model represents soft clay that tends to contract on cyclic loading, initially $H = 0$. The damage-hardening ($D - H$) domain is bounded by three values of undrained strength – an initial value, s_{u0}, an initial minimum value, $s_{u,min}$, and a final fully-hardened value, $s_{u,max}$.

Consolidation causes densification and hardening through the dissipation of pore pressure and this is captured in the model by a time-dependent reduction in the damage index concurrent with an increase in the hardening index. This is analogous to consolidation following an unload-reload path, and the slope of this hardening path is defined by κ^* (Fig. 1b Panel D).

The minimum strength is defined by as $s_{u,min} = s_{u0}/S_{t0}$ where S_{t0} is the initial soil sensitivity. As the soil densifies, the sensitivity reduces to unity and the strength converges to $s_{u,\ max}$, which is related to s_{u0} by the compression index parameter λ^*. The parameter λ^* is the slope of the line when damage D=0 (Fig. 1b, Panel D) and is analogous to the slope of the critical state line, which is also linked to the potential change in soil strength from densification.

3.2. Model formulation

The current normalised strength $\left(\frac{s_u}{s_{u0}}\right)$, where s_{u0} is the initial undrained strength, depends on the current hardening (H) and damage (D). The equilibrated strength (s_{ue}) is a strength at the current H when D=0

$$\frac{s_{ue}}{s_{u0}} = 1 + \frac{H}{\lambda^*} \tag{6}$$

The current strength (s_u) is therefore

$$\frac{s_u}{s_{ue}} = 1 - D\left(1 - \frac{1}{S_t}\right) \tag{7}$$

and the current normalised strength $\left(\frac{s_u}{s_{u0}}\right)$ can be found from combining Eqs. (6) and (7).

A general form of the geometry of the model, shown in Fig. 1 allows the sensitivity, S_t, to fall as hardening increases from $S_t = S_{t0} \rightarrow 1$ as $H = 0 \rightarrow 1$, at a set rate by the power of a constant, q:

$$S_t = 1 + (S_{t0} - 1)(1 - H)^q \tag{8}$$

Therefore, no pore pressure generation will occur once $H = 1$. At this point, the soil has reached a (cyclic) critical state, $S_t = 1$ and the damage and hardening process stop. In an initial burst of cyclic loading, taking place over a short time period such that consolidation and hardening is minimal, $D \rightarrow 1$, $H = 0$ so $s_u \rightarrow s_{u,min}$. In the long term, as consolidation dominates, $H \rightarrow 1$ so $s_u \rightarrow s_{u,max}$ so long as there is cyclic loading causing damage, from which consolidation can create a gain in strength. s_{uR} is the ratio between the maximum and initial soil strengths $s_{u,max}/s_{u0}$ and is found from Eq. (6) when H=1, so that $s_{uR} = 1 + 1/\lambda^*$.

3.3. Damage and hardening

Increases in damage during the period of a sea state are calculated via the *RSN* method and cannot exceed D=1. This damage also decays with time due to pore pressure dissipation, leading to consolidation. The rate of this decay follows the typical scaling of consolidation, being proportional to the ratio of the coefficient of consolidation and diameter of the anchor, $\frac{c_v}{B^2}$:

$$\frac{dD}{dt} = -k_{d2}\frac{c_v}{B^2}D^{\beta} \tag{9}$$

where k_{d2} and β are dimensionless parameters, enabling flexibility for the solution to be scaled to match analytical solutions for the dissipation of pore pressures (e.g. for plates, based on Gourvenec et al. 2010)

The increment of hardening is related to the damage dissipated and is expressed by modifying Eq. (9):

$$\frac{dH}{dt} = k_{d2}(1 - H)^{\gamma}\frac{\kappa^* c_v}{B^2}D^{\beta} \tag{10}$$

such that consolidation leads to hardening, following a path in the H vs $\frac{s_u}{s_{u0}}$ space, dependent on κ^*. κ^* sets the initial slope of the hardening response at H=0 and lies in the range of 0 to 1. The parameter γ sets how this slope changes as $H \rightarrow 1$. The dimensionless parameters q, k_{d2}, β and γ have been obtained by fitting the RSN—CSI model's response to measured model-scale foundation responses, as well as from theoretical solutions. They may not be strongly influenced by soil parameters, so could be applicable to other conditions, but further work is needed to identify links between soil properties and these model parameters. This is discussed in further detail in Section 5.

The combined effects on D of accumulation (from a set of loads analysed using the RSN model) and dissipation (from consolidation over time), means that the analysis proceeds in time steps over which any reduction in D due to consolidation is small. This is required because changes in D affect s_u, which in turn affect R and S because these dimensionless quantities involve normalising the anchor load by the current anchor capacity.

4. Anchor capacity

The soil strength is linked to the anchor capacity using a conventional bearing capacity approach. For this paper, it is assumed that the anchor is buried sufficiently deeply that a local failure mechanism is mobilised, with soil flow around the anchor. In this case the capacity is independent of the burial depth, and is given by:

$$Q_{ult} = N_c s_u A_p \tag{11}$$

where N_c is the bearing factor (with 12.42 being the theoretical value for a smooth thin embedded circular plate (Martin et al., 2001)), s_u is the current undrained soil strength and A_p is the plate area.

This study uses the following two assumptions to capture, in an efficient way, the changes in anchor bearing capacity caused by the loading and consolidation processes:

1 s_u is modelled as a single representative strength around the anchor, which varies as a result of the applied loading and consolidation according to the RSN—CSI model
2 N_c depends on the geometry of the plate and is assumed to be constant throughout the analysis.

The first assumption effectively 'smears' any spatial variations in strength change around the anchor and the second overlooks any changes in the failure mechanism. Various studies, using data from model tests and numerical analysis, have shown that changes in bearing capacity can be reliably assessed based on these two assumptions (albeit using relationships other than RSN—CSI for the effect of loading on s_u) (Bransby 2002; Stanier et al. 2019; Gourvenec et al., 2014; Feng et al. 2015, Peccin da Silva et al. 2021). The Stanier et al. (2019) study specifically addresses the validity of these assumptions, exploring the spatial changes in strength and failure mechanism. Other studies have demonstrated the same form of behaviour, except that in their interpretation s_u has been held constant at the initial value, s_{u0}, and N_c has been assumed to vary with the applied loading (Stanier et al., 2014). In all cases, the general conclusion is that changes in bearing capacity due to variations in the strength of the surrounding clay can be captured well by varying a single scalar parameter – s_u or N_c – in accordance with the applied load and any consolidation period, without needing to explicitly model the spatial variations in strength.

5. Application to centrifuge model tests

The RSN—CSI model is first compared to changes in strength observed in two types of centrifuge model test that involved episodic cyclic loading in soft normally-consolidated clayey soils:

- T-bar penetrometer tests in soft kaolin clay reported by O'Loughlin et al. (2020)
- Plate anchor tests reported in normally-consolidated carbonate silt by Zhou et al. (2020)

The T-bar tests were unusual load-controlled episodic cyclic tests. The longest of these tests involved three sets of 20 cycles (to 75% of the initial capacity), with two intervening consolidation periods, following by a final penetration to measure the available soil strength. The other tests were curtailed versions of this longer test, therefore providing a measure of the soil strength at earlier stages (see O'Loughlin et al. 2020 for full details). The plate anchor test involved a sequence of 5 episodes of constant-amplitude load cycles, again interspersed with consolidation periods, following by a final pull to failure.

The RSN—CSI model parameters used to simulate these tests are summarised in Tables 1 and 2 and are also similar to the parameters adopted in White et al. (2022) which were used to fit centrifuge tests on a model pile . The procedure for simulating the T-bar and plate anchor tests uses the model elements described earlier, stepping forward in time. The RSN method is used to calculate the damage during each packet of cyclic loads. The resulting damage is combined with the time-dependent dissipation over the associated time period within the CSI model. This leads to updated values of hardening and undrained strength. The analysis steps forward in time, with the updated strength being used for normalisation of the next sequence of loads, to find R and S. As the soil progressively strengthens, successive cycles at the same absolute load become less damaging, due to the reduction in R and S. The results for simulation of the T-bar test are shown in Fig. 2, and the plate anchor results are shown in Fig. 3.

The calculated changes in strength throughout the T-bar test follow closely the five measured values from the end of the longest test and the curtailed tests (Fig. 2a). The strength decreased during the 20 cycles of each loading stage as the damage rate exceeded the dissipation, but during the consolidation periods a high recovery of strength is simulated

Table 1
Summary of framework parameters used in the simulation of centrifuge model T-bar test in kaolin. Further details can be found in O'Loughlin et al. (2020).

Framework component	Parameter	Description	Value	Remarks
Geometry	B	T bar diameter (prototype scale)	0.75 m	Bearing capacity factor, N_c = 12.56 Einav et al. (2005)
Loads	S	Cyclic amplitude load ratio	0.5	Selected from cyclic loads O'Loughlin et al. (2020) for an applied number of cycles, N=20
	R	Average cyclic load ratio	0.5	
	t_{cyc}	Duration of cyclic loads	1 day	At full scale
	t_c	Duration of intervening consolidation stage	6.5 years	
Soil Characteristics	γ'	Effective unit weight	6.7 kN/m^3	O'Loughlin et al. (2020)
	S_{t0}	Initial soil sensitivity	2.5	Measured by cyclic T-bar test O'Loughlin et al. (2020)
	c_v	Coefficient of consolidation	2.6 m^2/year	Measured by piezocone tests (Chow et al., 2020; O'Loughlin et al. (2020)
Critical state model	λ^*	Compression index	0.385	Slope of D=0 line (Fig. 1b Panel D)
	κ^*	Swelling index	0.36	Slope of hardening path (Fig. 1b Panel D)
	$(s_u/\sigma'_{v0})_{NC}$	Normally consolidated undrained strength ratio	0.275	Based on an undrained shear strength gradient k=1.76 kPa/m and effective unit weight 6.7 kN/m^3
Pore pressure accumulation	k_1		1.0	Selected to provide RSN curves similar to those presented for Drammen clay in Andersen (2015)
	k_2		1.4	
	k_3		4	
	k_4		0.05	
	k_5		1	
Hardening/dissipation	k_{d2}	Dimensionless parameter	1	Fit to match model results
	β	Dimensionless parameter	1	From consolidation solution (Osman and Randolph, 2012)
	q	Rate of decrease in sensitivity as hardening increases	0.3	Fit to match model results
	γ	Rate of change in hardening as $H \rightarrow 1$	2.8	Fit to match model results

Table 2
Summary of framework parameters used in the simulation of centrifuge model plate anchor tests in natural carbonate silt. Further details can be found in O'Loughlin et al. (2020) and Zhou et al. (2020).

Framework component	Parameter	Description	Value	Remarks
Geometry	B	Diameter of circular plate anchor (prototype scale)	5.25 m	Bearing capacity factor, N_c = 12.42 Martin et al. (2001)
Loads	S	Cyclic amplitude load ratio	0.5	Selected from cyclic loads O'Loughlin et al. (2020) for an applied number of cycles, N=1080
	R	Average cyclic load ratio	0.5	
	t_{cyc}	Duration of cyclic loads	40 weeks	At full scale
	t_c	Duration of intervening consolidation stage	7.5 years	
Soil Characteristics	γ'	Effective unit weight	5.2 kN/m^3	Zhou et al. (2020)
	S_{t0}	Initial soil sensitivity	5	Measured by cyclic T-bar test O'Loughlin et al. (2020), Zhou et al. (2020)
	c_v	Coefficient of consolidation	3.5 m^2/year	Measured by piezocone tests (Chow et al., 2020; O'Loughlin et al. (2020)
Critical state model	λ^*	Compression index	0.4	Slope of D=0 line (Fig. 1b Panel D)
	κ^*	Swelling index	0.25	Slope of hardening path (Fig. 1b Panel D)
	$(s_u/\sigma'_{v0})_{NC}$	Normally consolidated undrained strength ratio	0.385	Based on an undrained shear strength gradient k=1.84 kPa/m and effective unit weight 5.2 kN/m^3
Pore pressure accumulation	k_1		0.8	Selected to provide RSN curves similar to those presented for Drammen clay in Andersen (2015)
	k_2		1.4	
	k_3		4	
	k_4		0.05	
	k_5		1	
Hardening/dissipation	k_{d2}	Dimensionless parameter	1	Fit to match model results
	β	Dimensionless parameter	1	From consolidation solution (Osman and Randolph, 2012)
	q	Rate of decrease in sensitivity as hardening increases	0.3	Fit to match model results
	γ	Rate of change in hardening as $H \rightarrow 1$	1.4	Fit to match model results

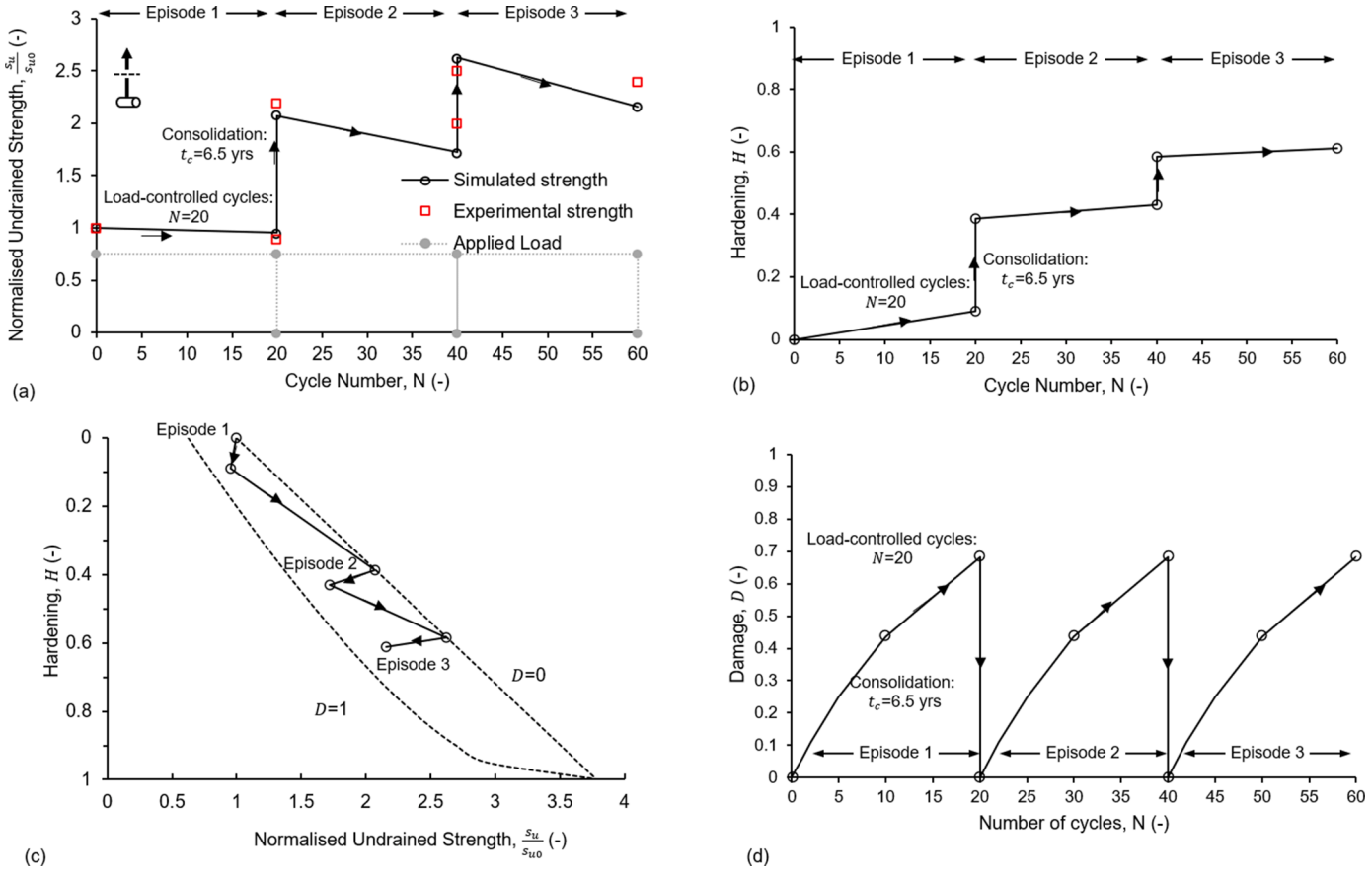

Fig. 2. Comparison of predicted and experimental soil responses during episodic T-bar centrifuge tests.

and measured. The final soil strength is more than double the initial value. The evolution of damage and hardening are also shown in Fig. 2b, c and d, illustrating the model behaviour.

The calculated change in strength over the loading period during the episodic cyclic plate anchor test is also closely predicted (Fig. 3). In this test, each cyclic packet consisted of a larger number of cycles – 1080 – and the damage approached the limit of $D = 1$ over this period, although the capacity always remained above the applied load. Each

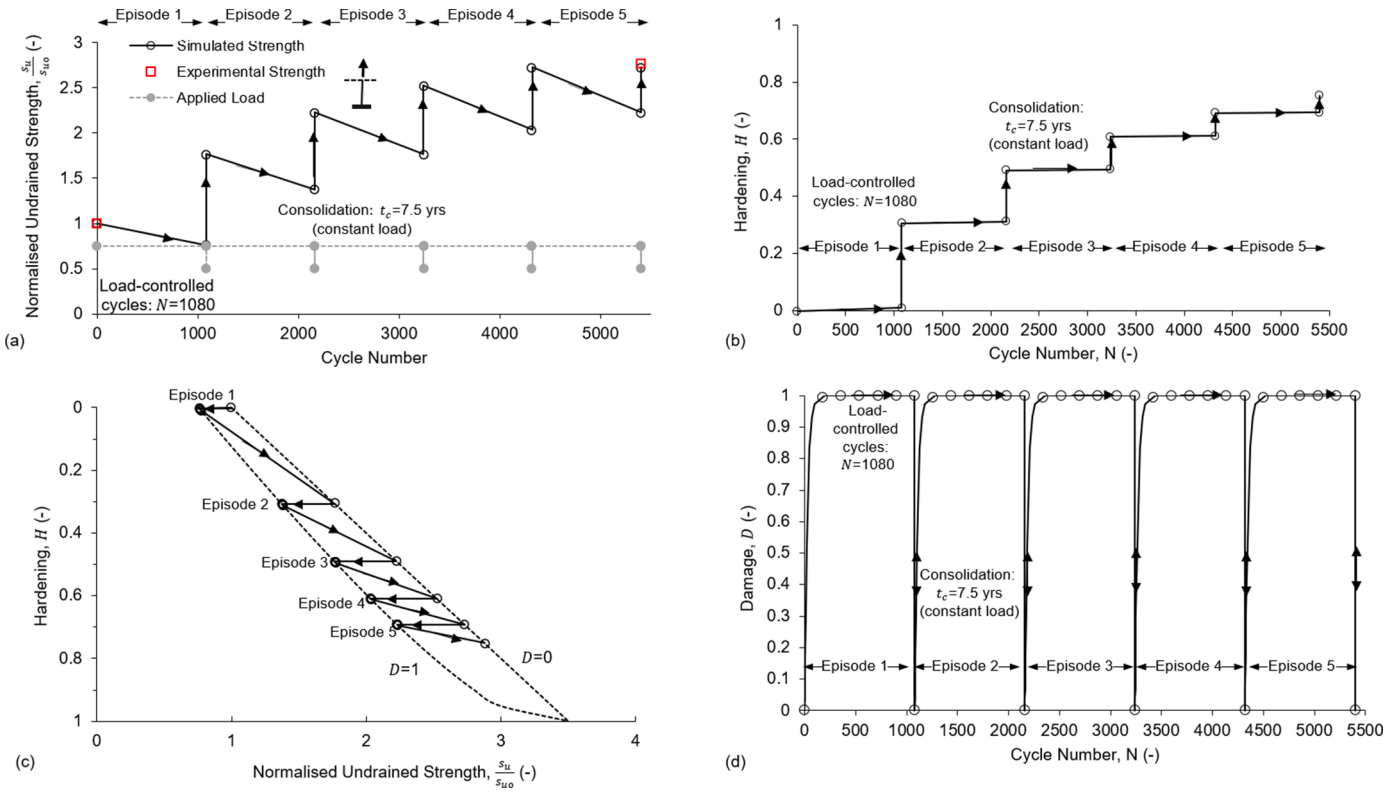

Fig. 3. comparison of predicted and experimental soil responses during episodic plate anchor centrifuge tests.

consolidation period led to a gain in strength, with the final anchor capacity being 2.7 times the initial capacity measured in a separate comparison test. The evolution of damage and hardening follow a similar zig-zag path for both the T-bar and plate anchor cases, converging towards the final strength given by $s_{u,max}$ as $H \rightarrow 1$.

The two comparisons illustrate the model behaviour and show promising agreement with the trends observed in model testing of two different foundation types in two different soils, using only a single set of model parameters. Both model tests involved discrete consolidation episodes and simple constant-amplitude cyclic loading. In the following example, we apply the RSN—CSI model to more realistic patterns of cyclic loading, and over a longer period of analysis that represents multiple years of operation.

6. Application to offshore wave energy converter

6.1. Introduction

The load sequences experienced by anchoring systems connected to floating infrastructure involve a spectrum of cyclic amplitudes and mean values, with this spectrum varying with metocean and operational conditions. This section describes the methodology used to simulate the anchor loads due to seasonally-varying sea states acting on a particular type of taut line wave energy converter (WEC) – the XMED buoy. This buoy was designed as a generic representation of a heaving point absorber and has characteristics that are typical of full scale WECs (Hann et al., 2015). This methodology is then applied using a Monte Carlo approach to assess the probability of failure and system reliability – with and without the whole-life effects captured by the RSN—CSI model.

6.2. Characterisation of cyclic anchor loads

A Wave Energy Converter Simulator (WEC-Sim) model of the XMED wave energy converter (Hann et al., 2015, 2018; Tosdevin et al., 2020) was used to simulate three-hour sets of continuous force-time cyclic anchor loads based on a range of sea states with varying likelihood, defined by selected pairs of significant wave height (H_s) and peak wave period (T_p) as shown in Fig. 4a. The environmental contours in Fig. 4a define the likelihood of a sea state according to the IFORM method (DNV 2019) and are based on 40 years of hindcast data from the Wave Hub site (NNRCMP, 2022), located 16 miles off Hayle, on the north coast of Cornwall, UK.

The "rainflow" counting method was used to identify the peaks and troughs in the force-time series to find the average cyclic and cyclic amplitude loads in each half-cycle, which are then converted to cyclic amplitude (S) and average cyclic (R) load ratios Fig. 1 Panel B) as defined in Eqs. (4) and ((5). For each sea state, the cyclic loads were grouped and binned into a 3D load histogram summarising the number of cycles (N) of a particular range of mean and cyclic load components, $F_{,avg}$ and F_{amp}. Therefore, each sea state defined by an H_s, T_p pair in Fig. 4a has a corresponding set of anchor loads that are specific to the XMED buoy and the maximum loads for each sea state pair are summarised in Fig. 4b. Therefore, an anchor load histogram can be interpolated for any H_s, T_p pair in the region defined by the environmental contour defining a 1 in 100-year likelihood, using the current s_u.

To create a realisation of the long-term anchor loading (i.e. a continuous operational lifetime anchor loading history), seasonally varying sea states were randomly sampled using a conditional modelling approach (CMA) as specified in the DNV code (DNV 2019). Monthly joint probability density functions (PDFs) were fitted to match the distributions of H_s and T_p, in the 40 years of hindcast data. The monthly marginal distribution of H_s was modelled by a 3-parameter Weibull PDF as defined in the equation below

$$f_{H_s}(h) = \frac{\beta_{H_s}}{\alpha_{H_s}}\left(\frac{h-\gamma_{H_s}}{\alpha_{H_s}}\right)^{\beta_{h_s}-1} \exp\left(-\left(\frac{h-\gamma_{H_s}}{\alpha_{H_s}}\right)^{\beta_{h_s}}\right) \tag{12}$$

where α_{H_s}, β_{H_s} and γ_{H_s} are scale, shape and location constants that define the 3-parameter Weibull PDF. The peak wave period (T_p) conditional on H_s was modelled by a lognormal distribution as defined below

$$f_{T_p|H_s}(t|h) = \frac{1}{\sigma t\sqrt{2\pi}} \exp\left(-\frac{(\ln t - \mu)^2}{2\sigma^2}\right) \tag{13}$$

where σ and μ are the shape and scale constants for the lognormal PDF. Therefore, to define the monthly joint PDFs for H_s and T_p, 12 sets of α_{H_s}, β_{H_s} and γ_{H_s} were fitted based on the recorded H_s data, specific to the month of the year, and five sets of σ and μ were fitted based on the recorded T_p data for each month (total of 60 sets), conditional on its paired value with H_s.

6.3. Long term simulation approach

Each simulation created a 3-year history of loading using these joint PDFs as the basis for seasonal variation – captured through monthly distributions of $H_s$and T_p- in the random sampling of sea states as shown in Fig. 5a, b and c. Less severe sea states and therefore less onerous cyclic load populations are found in summer (mid-year) compared to winter (start and end of the year).

In this example application there is no coupling between the mooring system and the foundation, (i.e. the anchor's response to the applied

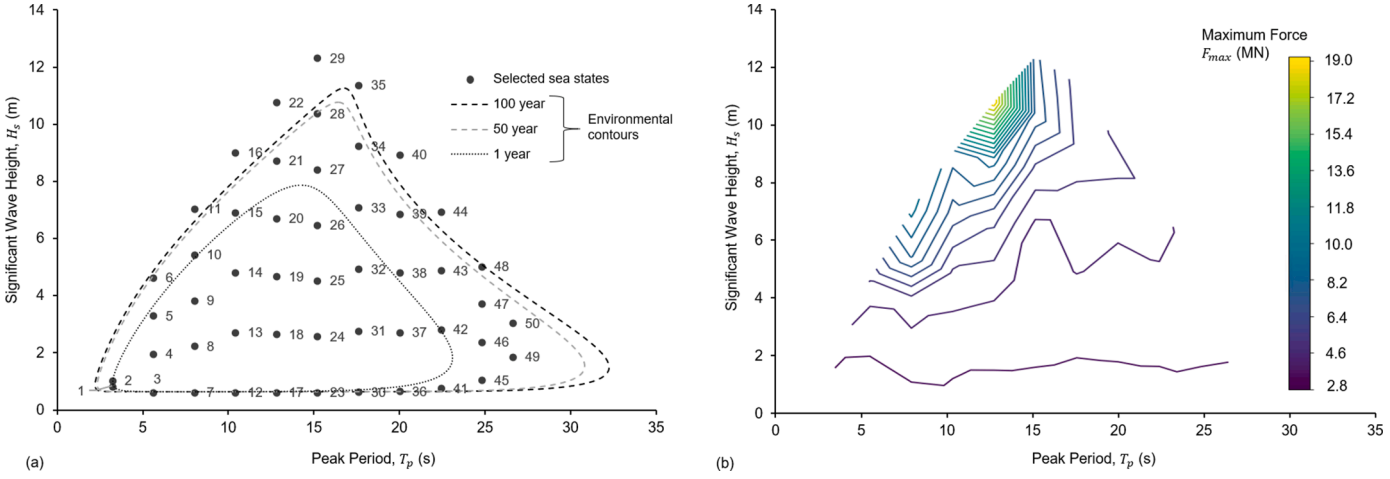

Fig. 4. (a) Simulated sea states and (b) resulting maximum peak anchor forces, F_{max} from a WEC-Sim analysis on the XMED wave energy converter.

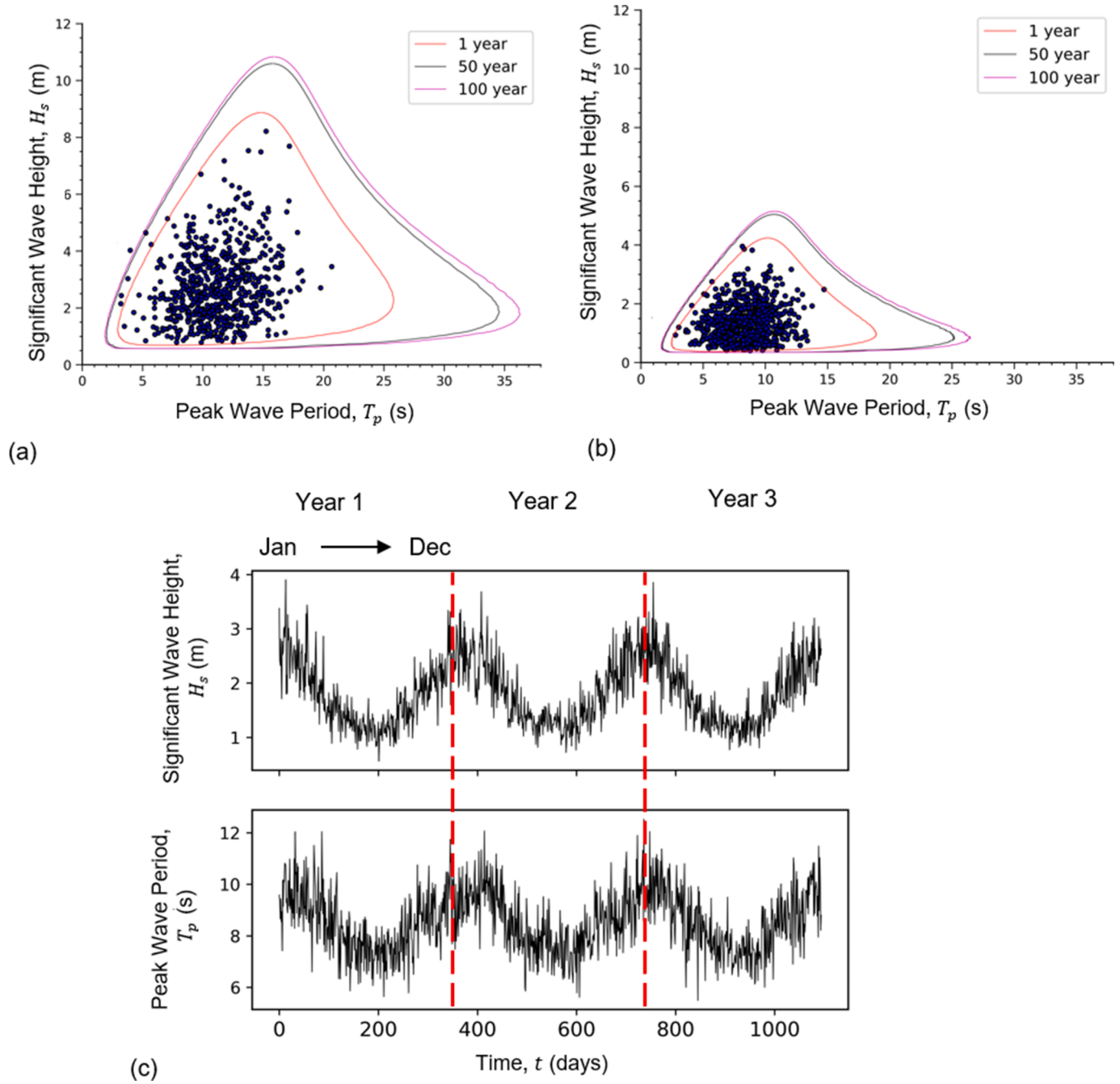

Fig. 5. Monthly seasonal variation in sea states selected during simulations: Typical sea states sampled at (a) the beginning of the year (January), (b) middle of the year (July) and (c) throughout the 3-year simulated time period.

loads has not effect on those loads) so the operational lifetime loading histories are generated independent of the foundation response. This uncoupled approach is usual for virtually all mooring analyses, as the seabed connection is usually modelled as a fixed pin. This assumption is reasonable unless the anchor compliance is non-negligible relative to the mooring line compliance, or the anchor reaches close to or beyond failure momentarily (as illustrated by Kwa et al., 2022).

Each operational lifetime starts at the beginning of the year, consists of a 3-year long sequence of 8760 × 3-hour sea states, with their associated cyclic loads. These are combined with the current s_u to generate an *RSN* distribution for each sea state, which leads to an updated damage, *D*. The CSI model parameters (*D* and *H*) are then updated after each 3-hour sea state. This timestep provides an efficient balance between two considerations: (i) it is long enough to provide much faster analysis than a cycle-by-cycle approach, in which each wave is modelled explicitly, and (ii) it is short enough that consolidation-related gains in undrained strength during the period can be neglected. For each sea state, the capacity after inclusion of any further damage is compared to the maximum anchor force, to identify whether anchor failure occurs.

The RSN—CSI model parameters used in the X-MED simulations are summarised in Table 3 and are based on previous parameters that were used to simulate the T-bar and plate anchor centrifuge tests in Section 5. The following sections describe simulation results for different sizes of circular plate anchors. A total of 10,000 simulations using different randomly-sampled 3 year-long sequences of 3-hour sea states were performed for each anchor size, to capture the random and seasonal variability in loading. Based on the number of simulations that indicated

Table 3
Summary of framework parameters used in the simulation of plate anchor used to anchor the X-MED wave energy buoy.

Framework component	Parameter	Description	Value	Remarks
Geometry	B	Diameter of circular plate anchor	5 m	Bearing capacity factor, N_c = 12.42 Martin et al. (2001)
Loads	S	Cyclic amplitude load ratio	Variable	Determined using WEC-Sim model of single line taut moored X-MED buoy
	R	Average cyclic load ratio	Variable	
Soil Characteristics	γ'	Effective unit weight	6.7 kN/m^3	O'Loughlin et al. (2020)
	S_{t0}	Initial soil sensitivity	2.5	Measured by cyclic T-bar test O'Loughlin et al. (2020); Zhou et al. (2020)
	c_v	Coefficient of consolidation	3.5 m^2/ year	Set to dissipate 10% of generated damage
Critical state model	λ^*	Compression index	0.4	Slope of D=0 line (Fig. 1b Panel D)
	κ^*	Swelling index	0.25	Slope of hardening path (Fig. 1b Panel D)
	$(s_u/\sigma'_{v0})_{NC}$	Normally consolidated undrained strength ratio	0.275	Based on an undrained shear strength gradient k=1.76 kPa/m and effective unit weight 6.7 kN/m^3
Pore pressure accumulation	k_1		1.0	Selected to provide RSN curves similar to those presented in Andersen (2015)
	k_2		2.8	
	k_3		4	
	k_4		0.05	
	k_5		1	
Hardening/dissipation	k_{d2}	Dimensionless parameter	1	Fit to match model centrifuge results
	β	Dimensionless parameter	1	From consolidation solution (Osman and Randolph, 2012)
	q	Rate of decrease in sensitivity as hardening increases	0.3	Fit to match model centrifuge results
	γ	Rate of change in hardening as $H \rightarrow 1$	2.8	Fit to match model centrifuge results

anchor failure, these results lead to estimates of the system reliability.

The calculations are implemented in Python and run on an Ubuntu (Linux) operating system. A single simulation takes <5 s, and many simulations can be run concurrently on a single workstation.

6.4. Simulation results from base case ($B = 5m$) single analyses

The model behaviour is first illustrated using a single simulation with a base case anchor diameter of $B = 5m$ (Fig. 6). High damage was generated during the first 3 months of the simulation, but as the soil hardened and the season became summer, with low loads, the damage level reduced. A minimum current strength of $\sim 0.5 s_{u0}$ occurred during the first month, although this remained above the minimum value of $s_{u,min} = 0.41 s_{u0}$ for the adopted parameters, and also above the mobilised strength ($s_{u,mob} = \frac{F_t}{N_c A_p}$) which is the minimum soil strength required to resist external forces that is based on the applied anchor loads. After 6 months, the current undrained strength s_u was approximately double s_{u0} due to consolidation.

During subsequent winters, damage accumulates again, but the strength remained higher during the first winter, reflecting the reduced sensitivity, S_t and higher H, as illustrated by the CSI model path shown in Fig. 7.

Simulations were also performed with soil hardening disabled, by setting $\kappa^* = 0$. In these simulations, the dissipation of damage caused regains in soil strength limited to $s_u = s_{u0}$, as shown in Fig. 6d, f and by the horizontal path at $H = 0$ for values of damage $0 < D < 1$ in Fig. 7. High damage was sustained because of R and S remaining high, compared to the hardening case in which R and S reduce due to the rise s_u.

6.5. Simulation results from larger anchor ($B = 7.5m$) analyses

Similar but less dramatic trends in soil strength and hardening are observed for a larger anchor diameter (B=7.5 m) (Figs. 8 and 9). This is because the applied average cyclic load and cyclic amplitude load ratios (R and S) are smaller for larger anchor diameters. This results in lower

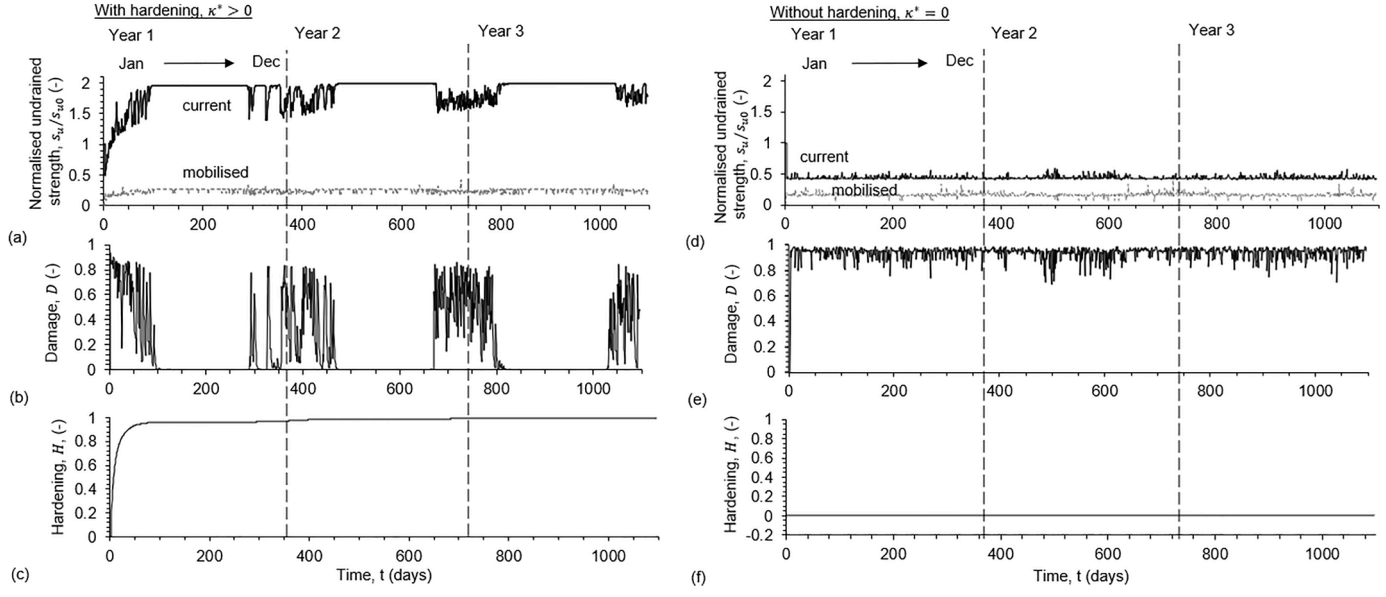

Fig. 6. Comparison of soil (a, d) strength, (b, e) damage, (c, f) hardening responses with and without hardening for an anchor diameter B=5 m.

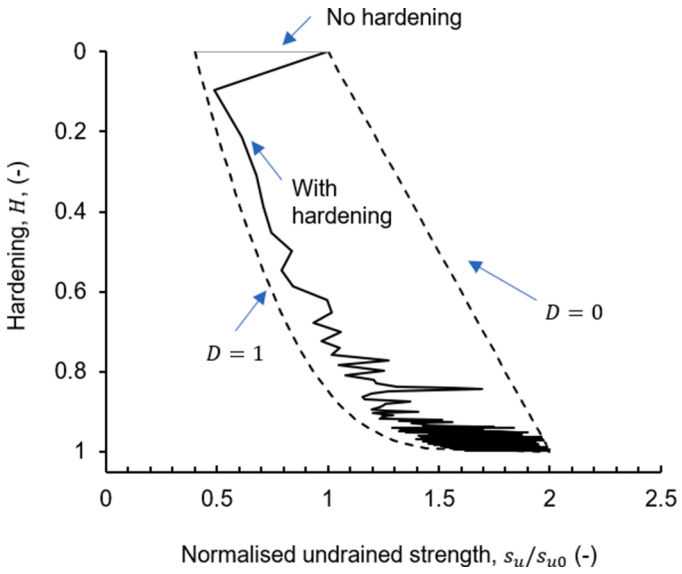

Fig. 7. Comparison of soil hardening versus strengthening responses without and without hardening for an anchor diameter B=5 m.

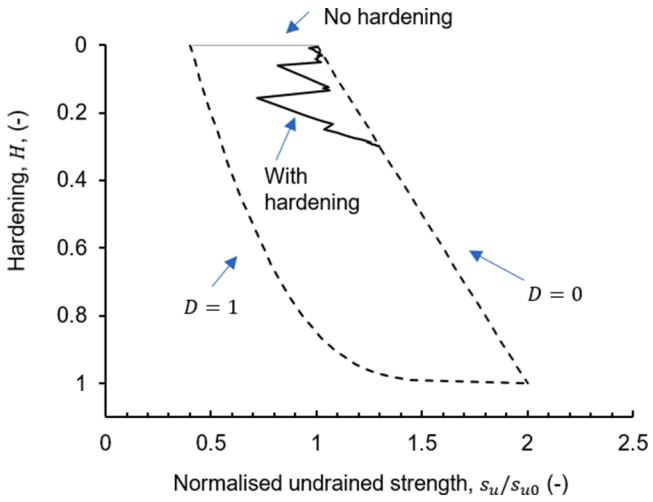

Fig. 9. Comparison of soil hardening versus strengthening responses without and without hardening for an anchor diameter B=7.5 m.

applied accumulated damage, and so smaller changes in current strength and hardening (according to Eqs. (7) and (10). Damage was only generated during the first winter, leading to hardening until $s_u \sim 1.3\, s_{u0}$ (Fig. 8b). This gain in strength was sufficient for subsequent winters to cause zero damage (Fig. 8c). With hardening switched off, each winter causes damage and a reduction in strength, which is then recovered during summer (Fig. 8d, e).

6.6. Monte carlo simulation results for base case anchor ($B = 5m$)

A total of 10,000 simulations were performed for each anchor size, leading to collated time histories of s_u, D and H, with and without hardening. The 90th, 50th and 10th percentile (P_{90}, P_{50}, P_{10}) responses of these parameters indicate the range of damage and hardening responses, caused by the loading variation from random sampling of sea states.

The results for the base case anchor ($B = 5m$) are shown in Fig. 10. The winter period, when rare but severe sea states can occasionally occur, leads to a higher variation between the P_{10} and P_{90} values of D and s_u/s_{uo}. The pattern of winter damage repeats each year, but the hardening in each winter causes the changes in strength during subsequent years to be reduced. In all cases, the gain in strength during the first year creates a high margin of safety between the mobilised and available strength throughout subsequent winters. When hardening is disabled ($\kappa^* = 0$) the range of each parameter is smaller, and each winter leads to a convergence between the mobilised and available strengths.

The results for the larger anchor ($B = 7.5m$) are shown in Fig. 11. In this case only the first winter causes damage to be mobilised, with a wide range observed: the peak of the P_{90} profile is ~0.8, whereas the P_{10} profile does not exceeds 0.05. Consequently, the hardening and strength gain after the first winter both vary, with the long-term strength in the range s_u/s_{uo}= 1.3 – 1.6 ($P_{10} - P_{90}$). Without hardening, high values of damage in the range 0.5 – 0.9 ($P_{10} - P_{90}$) are evident each winter.

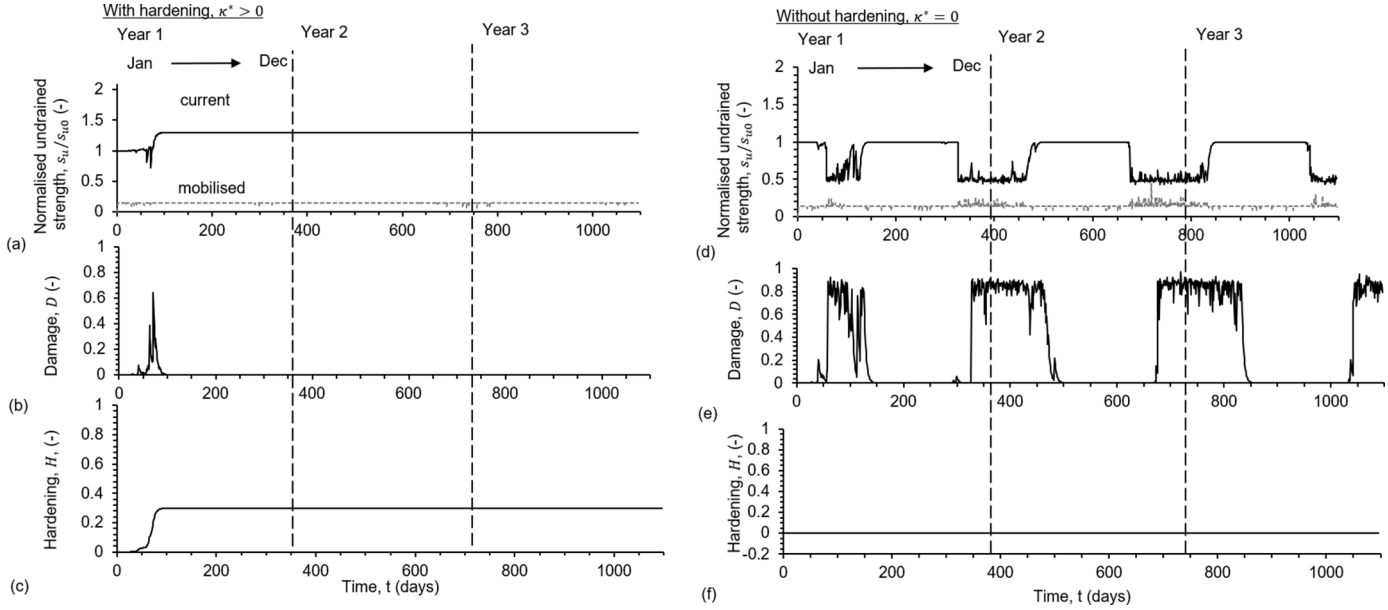

Fig. 8. Comparison of soil (a, d) strength, (b, e) damage, (c, f) hardening responses with and without hardening for an anchor diameter B=7.5 m.

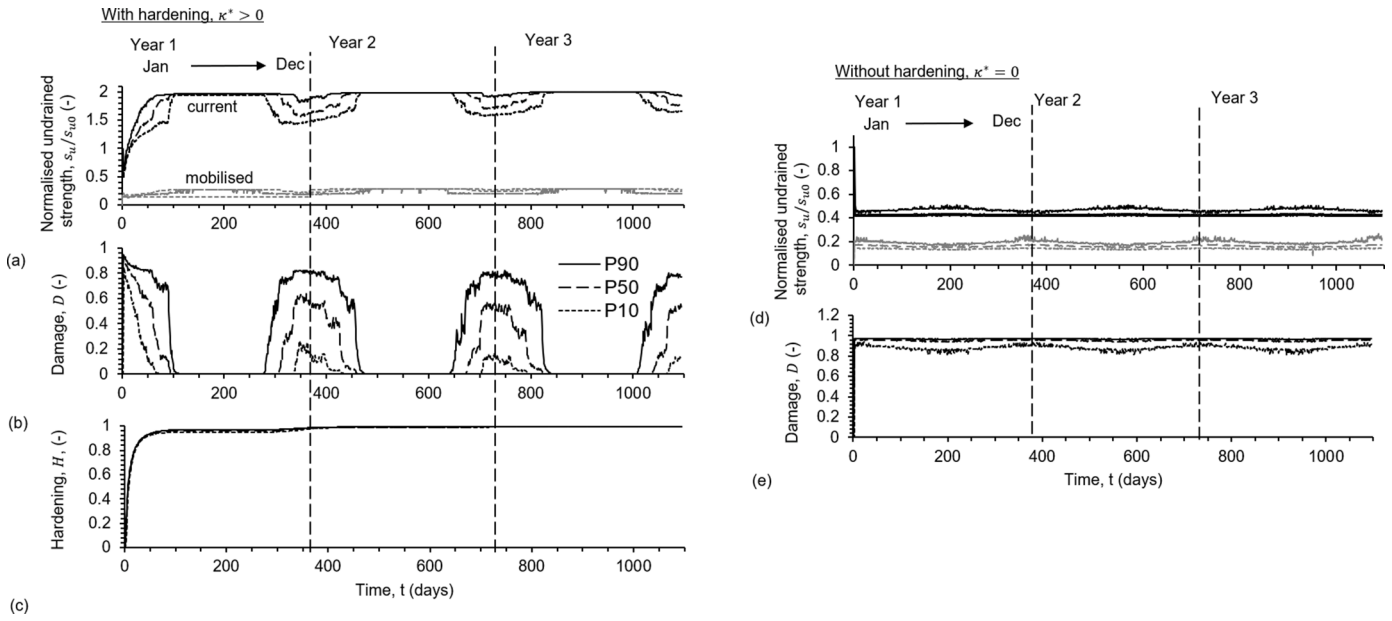

Fig. 10. Comparison of range in soil (a,d) strength, (b, e) damage and (c) hardening responses with hardening enabled and without hardening enabled for an anchor diameter B=5 m.

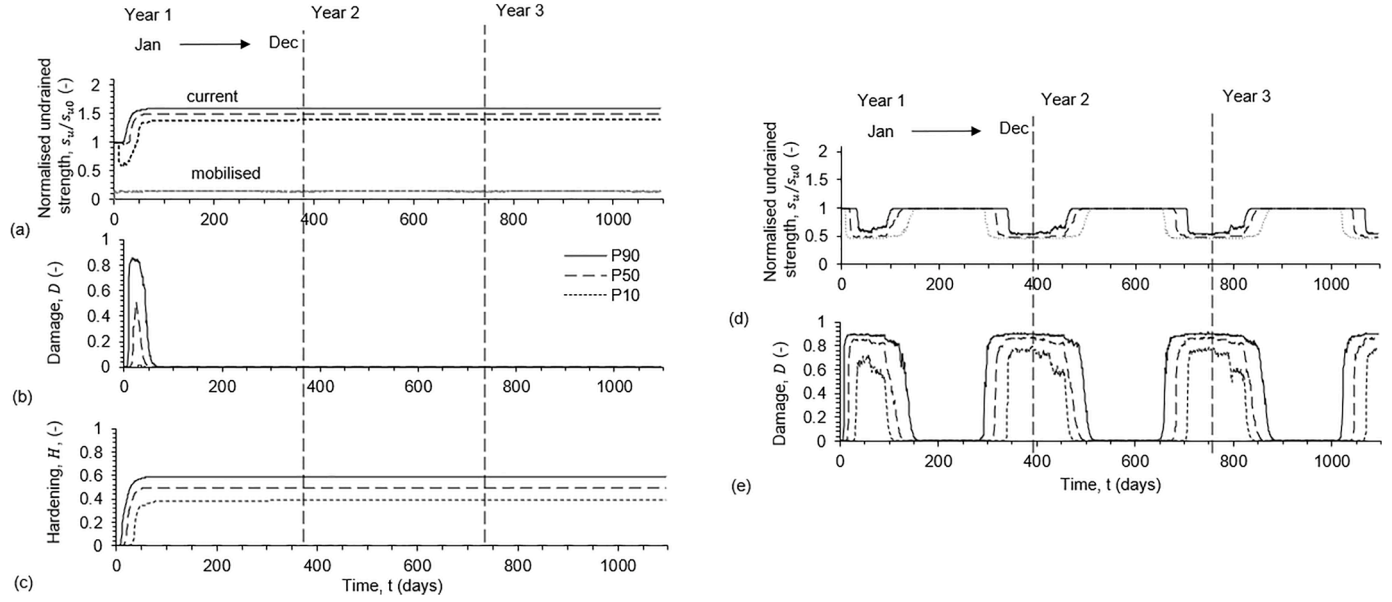

Fig. 11. Comparison of range in soil (a,d) strength, (b, e) damage and (c) hardening responses with hardening enabled and without hardening enabled for an anchor diameter B=7.5 m.

6.7. Reliability analysis: probabilities of failure

The 10,000 load history simulations were used to quantify anchor reliabilities for a range of anchor sizes and soil parameters, to allow for the uncertainty in the variable applied loads and the resulting changes in the anchor capacity from the RSN—CSI model. The soil conditions modelled in the reliability analyses are summarised in Table 4. The typical distribution of the maximum tension loads, F_{max}, applied during a realisation, as summarised in Fig. 12a and b, show that most of the maximum loads were from 14 to 17 MN and corresponded to sea states that were within the 1 in 100-year environmental contour. F_{max} was found from each realisation as

Table 4
Summary of anchor and soil parameters adopted during the reliability analyses.

Parameter	Values	Units
Anchor diameter, B	4.5 to 8	m
Maximum soil hardening ratio, $s_{u,max}/s_{uo}$	1.5, 2*, 2.5, 3	–
Coefficient of consolidation c_v	0.97, 1.89, 2.7*, 5.4	m^2/year

* Base case values.

$$F_{max} = N_c s_u A \left(\frac{S}{2} + R\right)_{max} \quad (14)$$

The distribution of F_{max} is not as smooth as the distribution of H_s and T_p (Fig. 4) due to the influence of the WEC system response – as evident

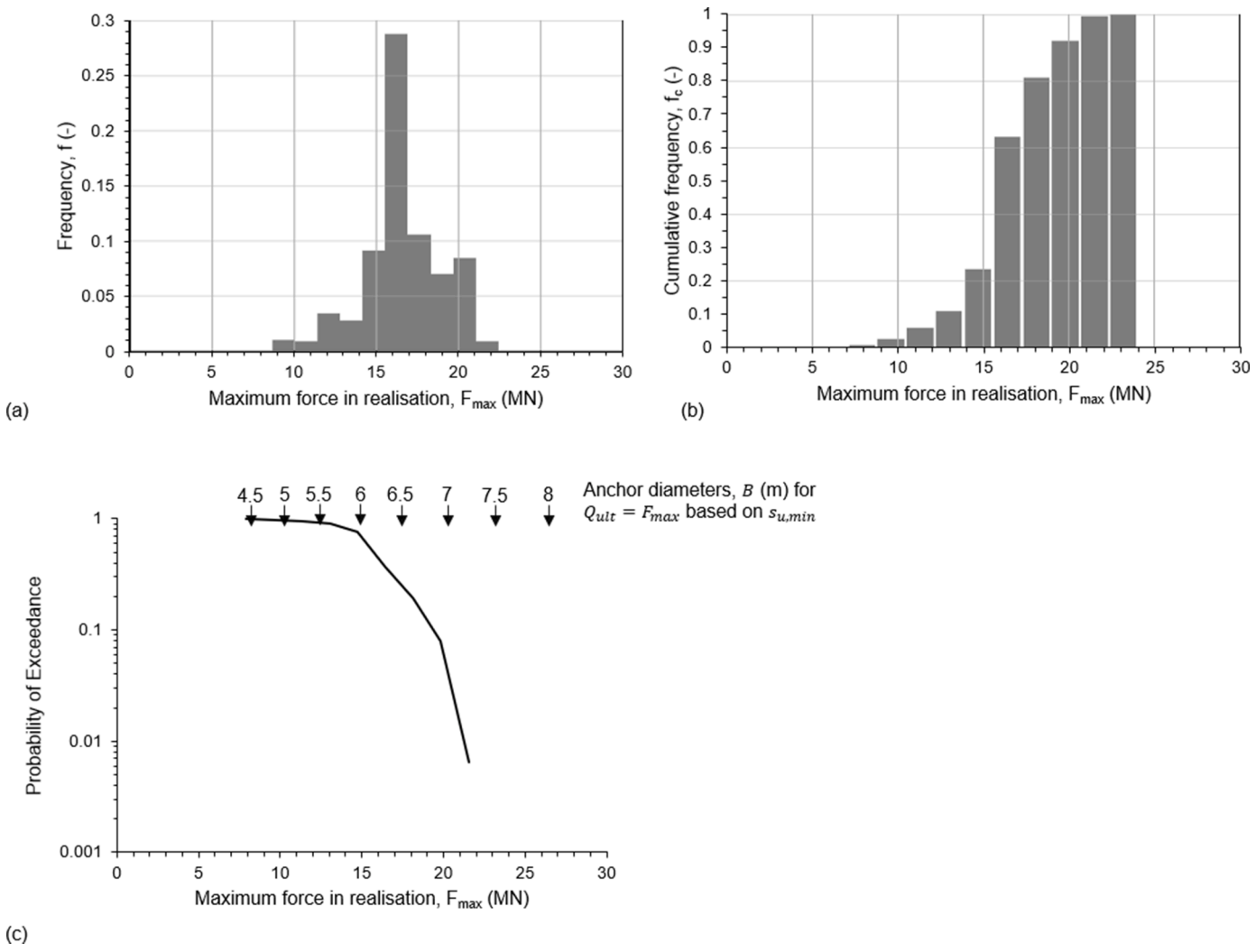

Fig. 12. Summary histograms showing (a) the distribution and (b) the cumulative distribution of the maximum forces, F_{max} in all realisations and (c) the probabilities of failure for anchor diameters for anchors embedded in soil at its minimum strength ($s_{u,\ min}$).

in the shape of the F_{max} distribution in Fig. 4b.

These maximum applied loads are presented as the probability of exceedance during the anchor lifetime in Fig. 12c. These loads are compared with the minimum anchor capacities to estimate a probability of anchor system failure (P_f) when the soil is set at the fully softened state (i.e. s_u is set to $s_{u,min}=\frac{s_{u0}}{S_{t0}}$ in Eq. (11)). Under this assumption, large anchor diameters, $B > 7.5$ m, are required to achieve a reference reliability of $P_f < 10^{-3}$.

However, smaller anchor diameters are required if the anchor capacity is assessed using the RSN CSI method, capturing whole-life changes in strength. The results for these analyses are summarised in Fig. 13. Each marker shows P_f based on 10^4 realisations, and the dotted lines are fitted to allow comparison of the anchor diameters required at the reference reliability of $P_f < 10^{-3}$.

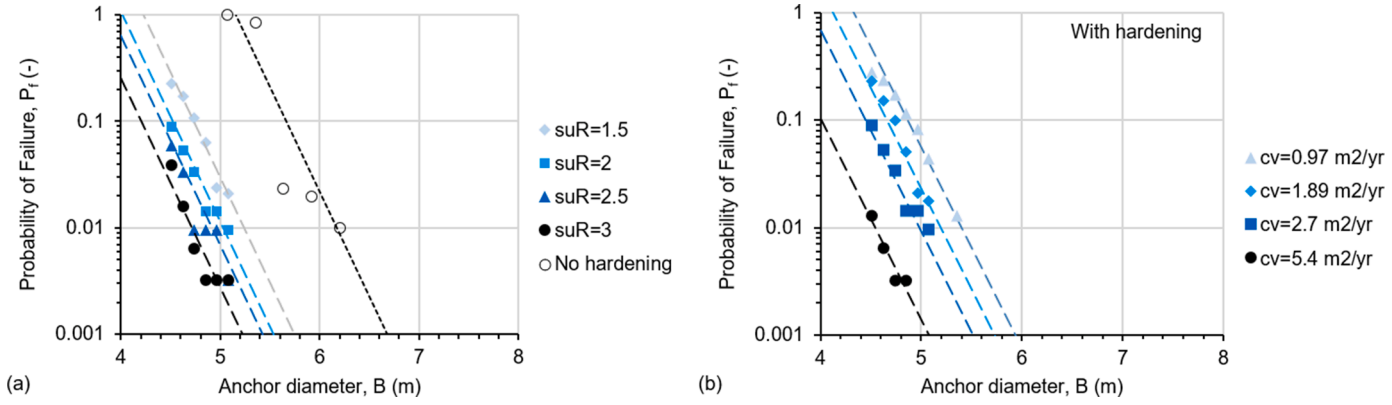

Fig. 13. Summary of the probability of failures for anchor diameters in (a) effect of varying s_{uR}, with and without hardening, (b) effect of varying c_v.

In this set of analyses, two soil parameters were varied: maximum soil strength increase, $s_{uR} = s_{u,max}/s_{u0}$, and the coefficient of consolidation, c_v, as summarised in Table 4. Also, cases with $\kappa^* = 0$ were performed, referred to as 'no hardening'. With no hardening, the required anchor size reduces slightly from the $s_{u,min}$ case, with diameters of B ~ 6.7 m required to achieve a $P_f < 10^{-3}$ (Fig. 13a). This improvement in the required anchor diameter is because the soil recovers due to consolidation and does not remain at its fully softened state, $s_{u,\ min}$. during cycling.

If hardening is enabled, larger reductions in the required anchor sizes can be made compared to the reference $s_{u,min}$ case. Within these cases, higher values of s_{uR} and c_v result in greater reductions in anchor diameter. A higher value for s_{uR} results in a higher potential undrained strength, while a higher value of c_v increases the rate of damage dissipation and soil hardening.

The reference probability of failure $P_f = 10^{-3}$ is a baseline used in Fig. 14 to compare the required anchor sizes with and without hardening and cyclic softening over a range of s_{uR} and c_v. The results show significant reductions in required anchor size, approximately halving the required cross-sectional area of the anchor (and therefore its weight) if beneficial strengthening and hardening soil effects are considered.

This halving of the required design anchor size predicted by the RSN—CSI model during these reliability analyses is consistent with centrifuge model test results on T-bar and plate anchors (O'Loughlin et al., 2020; Zhou et al., 2020) as well as direct simple shear test results (Laham et al., 2021). In all examples, an approximate doubling of strength or capacity was observed from the beneficial combined effects of cycles and consolidation.

7. Concluding comments

This study has shown that a novel macro-model approach – referred to as RSN—CSI can capture through-life changes in soft soil strength around embedded anchoring systems as a result of whole-life loading conditions. This allows beneficial consolidation effects as well as damaging cyclic effects to be combined, allowing the evolution in capacity to be compared with the varying load. The model combines established techniques of SN curves for damage and a critical state-inspired framework for hardening.

The model captures changes in soil strength seen in centrifuge experiments in which model T-bar penetrometers and plate anchors are subjected to cyclic loads with intervening consolidation. The model was also used to assess the through-life changes in soil response around an anchoring system connected to a single taut-moored wave energy converter. The simulations are fast, allowing Monte Carlo analysis of uncertainty in the sea states, loading history and evolution of soil strength. The observed gains in capacity compared to an analysis that neglects this beneficial recovery of soil strength indicate a potential halving of the required anchor area.

The approach provides a new basis for whole-life modelling of anchoring systems, capturing timescales from individual waves to annual seasons and soil consolidation. The method is sufficiently fast to allow reliability-based assessments via a Monte Carlo method. In soft soils that exhibit beneficial gains in capacity, this method provides a basis for more efficient design and can unlock reliability that is hidden in current designs.

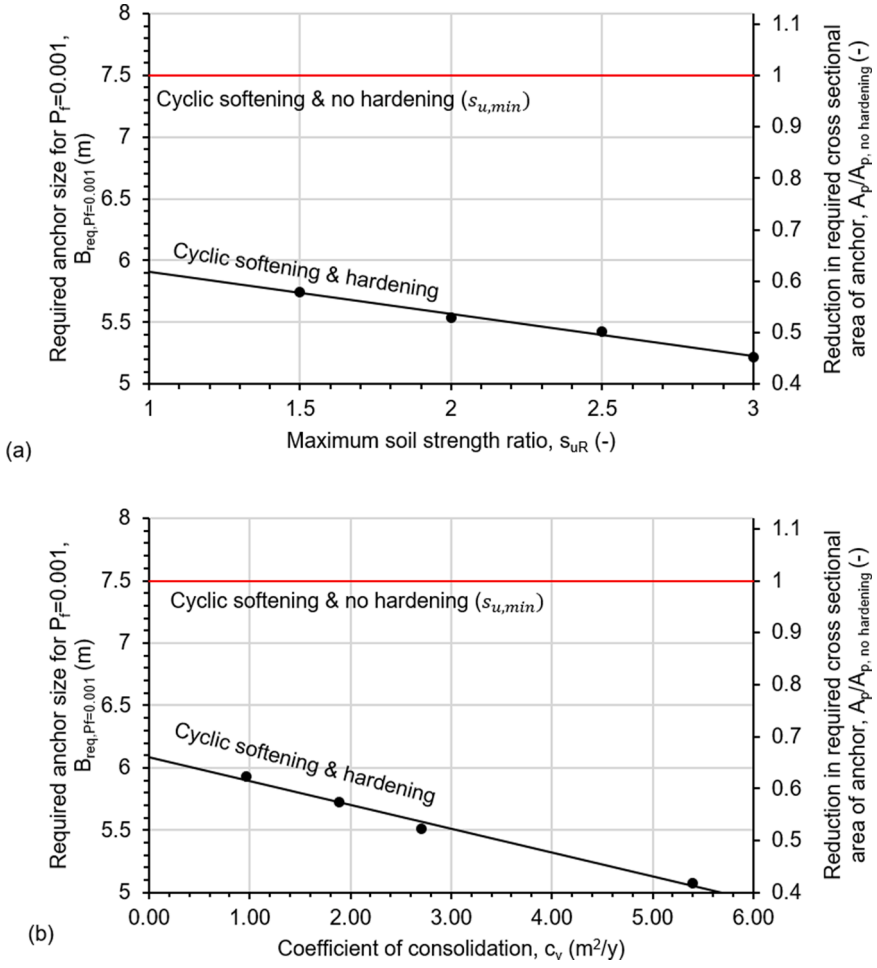

Fig. 14. Comparison of required anchor sizes for anchors embedded in (a) soil with varying strength, s_{uR} and (b) soil with different coefficients of consolidation, c_v.

CRediT authorship contribution statement

K.A. Kwa: Conceptualization, Methodology, Software, Validation, Formal analysis, Investigation, Data curation, Writing – original draft, Writing – review & editing, Visualization, Funding acquisition, Project administration. **D.J. White:** Conceptualization, Methodology, Formal analysis, Investigation, Writing – original draft, Writing – review & editing, Visualization, Funding acquisition, Project administration, Supervision. **T. Tosdevin:** Conceptualization, Methodology, Software, Data curation, Formal analysis, Writing – review & editing. **S. Jin:** Conceptualization, Methodology, Software, Data curation, Formal analysis, Writing – review & editing. **D. Greaves:** Conceptualization, Writing – review & editing, Funding acquisition, Project administration, Supervision.

Declaration of Competing Interest

The authors declare that they have no known competing financial interests or personal relationships that could have appeared to influence the work reported in this paper.

Data availability

Data will be made available on request.

Acknowledgments

This work forms part of research supported by the EPSRC Supergen Offshore Renewable Energy (ORE) Hub (Grant EPSRC EP/S000747/1) and by the Royal Academy of Engineering under the Research Fellowship Programme and the RAEng Chair in Emerging Technologies Centre of Excellence in Intelligent & Resilient Ocean Engineering (IROE).

References

Abadie, C.N., Byrne, B.W., Houlsby, G.T., 2019. Rigid pile response to cyclic lateral loading: laboratory tests. Géotechnique Vol. 69 (10), 863–876.
Andersen, K.H., 2009. Bearing capacity under cyclic loading—offshore, along the coast, and on land. The 21st Bjerrum lecture presented in Oslo, 23 november 2007. Can. Geotech. J. 46 (5), 513–535.
Andersen, K.H., 2015. Cyclic soil parameters for offshore foundation design. the third ISSMGE McClelland lecture. Front. Offshore Geotech. III 1, 5–82.
Andersen K.H., Lauritzen R., 1988. Cyclic bearing capacity analysis for Gravity Platforms; calculation procedure, verification by model tests, and application for the Gullfaks C platform.
Bai, Y., 2016. Marine Structural Design. Elsevier Science, UK, pp. 851–873.
Bayton, S.M., Black, J.A., Klinkvort, R.T., 2018. Centrifuge modelling of long term cyclic lateral loading on monopiles. Physical Modelling in Geotechnics. CRC Press, pp. 689–694.
Bonjean, D., Erbrich, C., Zhang, G., 2008. Pipeline Floatation Assessment in Liquefiable Soil. In: Offshore Technology Conference. OnePetro, Houston, Texas.
Bransby, M.F., Pande, G.N., Pietruszczak, S., 2002. The undrained inclined load capacity of shallow foundations after consolidation under vertical loads. In: Proceedings of the Numerical models in geomechanics 8th international symposium (NUMOG VIII. Rotterdam, Netherlands, eds. Balkema, pp. 431–437.
Cerfontaine, B., White, D.J., Kwa, K., Gourvenec, S.M., Knappett, J.A., Brown, M.J., 2023. Anchor Geotechnics For Floating Offshore wind: Current Technologies and Future Innovations. Ocean Engineering (In Press).
Cocjin, M., Gourvenec, S., White, D.J., Randolph, M.F., 2014. Tolerably mobile subsea foundations – Observations of performance. Géotechnique 64 (11), 895–909.
Cocjin, M., Gourvenec, S., White, D.J., Randolph, M.F., 2017. Theoretical framework for predicting the response of tolerably mobile subsea installations. Géotechnique 67 (7), 608–620.
Chow, S.H., O'Loughlin, C.D., Zhou, Z., White, D.J., Randolph, M.F., 2020. Penetrometer testing in a calcareous silt to explore changes in soil strength. Géotechnique 70 (12), 1160–1173.
DNV, 2019. Recommended Practice DNV-RP-C205, Environmental Conditions and Environmental Loads. Det Norske Veritas.
Einav, I., Randolph, M.F., 2005. Combining upper bound and strain path methods for evaluating penetration resistance. Int. J. Numer. Methods Eng. 63 (14), 1991–2016.
Feng, X., Gourvenec, S.M., 2015. Consolidated undrained load-carrying capacity of subsea mudmats under combined loading in six degrees of freedom. Géotechnique Vol. 65 (7), 563–575. https://doi.org/10.1680/geot.14.P.090.
Gourvenec, S.M., Vulpe, C., Murthy, T.G., 2014. A method for predicting the consolidated undrained bearing capacity of shallow foundations. Géotechnique 64 (3), 215–225.
Gourvenec, S., Westgate, Z., 2020. Whole-life geotechnical design: what is it? What's it for? So what? And what next?: keynote. In: Proceedings of the 4th International Symposium on Frontiers in Offshore Geotechnics. Deep Foundations Institute, ed., pp. 206–246.
Guevara, M., Doherty, J., Watson, P., White, D, Westgate, Z., 2020. Key features impacting soil-conductor lateral behaviour as illustrated by centrifuge tests. In: Proceedings of the 4th International Symposium on Frontiers in Offshore Geotechnics, , ed.1069. Deep Foundations Institute.
Han, C., Wang, D., Gaudin, C., O'Loughlin, C.D., Cassidy, M.J., 2016. Behaviour of vertically loaded plate anchors under sustained uplift. Géotechnique 66 (8), 681–693.
Hann, M., Greaves, D., Raby, A., 2015. Snatch loading of a single taut moored floating wave energy converter due to focussed wave groups. J. Ocean Eng. 96, 258–271.
Hann, M., Greaves, D., Raby, A., Howey, B., 2018. Use of constrained focused waves to measure extreme loading of a taut moored floating wave energy converter. Ocean Eng. 148, 33–42.
Hodder, M., White, D.J., Cassidy, M.J., 2013. An effective stress framework for the variation in penetration resistance due to episodes of remoulding and reconsolidation. Géotechnique Vol. 63 (1), 30–43.
Jardine, R., Puech, A., Andersen, K.H., 2012. Keynote address: cyclic loading of offshore piles: potential effects and practical design. Offshore Site Investigation and Geotechnics: Integrated Technologies-Present and Future. OnePetro, London, UK.
Kwa, K.A., Sivasithamparam, N., Deeks, A., White, D.J., 2022. A numerical macro model to simulate the whole life response of anchors for floating offshore renewable energy systems. In: Proceedings of the International Conference on Offshore Mechanics and Arctic Engineering, 85949. ASME. V009T10A003.
Laham, N., Kwa, K., Deeks, A., Suzuki, Y., White, D., Gourvenec, S., 2023. Changing Soil Response During Episodic Cyclic Loading in Direct Simple Shear Tests. Int. J. Offshore Polar Eng. 33 (01), 54–61.
Laham, N.I., Kwa, K.A., White, D.J., Gourvenec, S.M., 2021. Episodic simple shear tests to measure strength changes for whole-life geotechnical design. Géotech. Lett. 11 (1), 103–111.
Lai, Y., Wang, L., Hong, Y., He, B., 2020. Centrifuge modeling of the cyclic lateral behavior of large-diameter monopiles in soft clay: effects of episodic cycling and reconsolidation. J. Ocean Eng. 200. No.107048.
Martin, C.M., Randolph, M.F., 2001. Applications of the lower and upper bound theorems of plasticity to collapse of circular foundations. In: Proceedings of the 10th International Conference on Computer Methods and Advances in Geomechanics. Tucson, AZ, pp. 7–12. Jan.
Tosdevin, T., Giassi, M., Thomas, S., Engstrom, J., Hann, M., Isberg, J., Goteman, M., Ransley, E., Musliedlak, P., Simmonds, D., Greaves, D., 2020. On the calibration of a WEC-Sim model for heaving point absorbers. 13th European Wave and Tidal Energy Conference EWTEC, Napoli, Italy.
National Network of Regional Coastal Monitoring Programmes (NNRCMP), (2022), Realtime data-, Retrieved https://coastalmonitoring.org/realtimedata/?chart=75&tab=waves&range=day&disp_option=1&user_indate=&datum=chart </Dataset>.
O'Loughlin, C.D., Zhou, Z., Stanier, S.A., White, D.J., 2020. Load-controlled cyclic T-bar tests: a new method to assess effects of cyclic loading and consolidation. Géotech. Lett. 10 (1), 7–15.
O'Loughlin, C.D., White, D.J., Stanier, S.A., 2017. Plate anchors for mooring floating facilities–a view towards unlocking cost and risk benefits. In: Proceedings of the Offshore Site Investigation Geotechnics 8th International Conference, 978, pp. 978–986. Society for Underwater Technology.
Osman, A.S., Randolph, M.F., 2012. Analytical solution for the consolidation around a laterally loaded pile. Int. J. Geomech. 12 (3), 199–208.
Peccin da Silva, A., Diambra, A., Karamitros, D., Chow, S.H., 2021. A cyclic macro element framework for consolidation-dependent three-dimensional capacity of plate anchors. J. Mar. Sci. Eng. 9, 199. https://doi.org/10.3390/jmse9020199.
Randolph, M., Gourvenec, S., 2017. Offshore Geotechnical Engineering, 136. CRC press, p. 137.
Richards, I.A., Byrne, B.W., Houlsby, G.T., 2018. Physical modelling of monopile foundations under variable cyclic lateral loading. Physical Modelling in Geotechnics. CRC Press, pp. 737–741.
Richards, I.A., Byrne, B.W., Houlsby, G.T., 2020. Monopile rotation under complex cyclic lateral loading in sandw. Géotechnique 70 (10), 916–930.
Smith, V.B., White, D.J., 2014. Volumetric hardening in axial pipe soil interaction. In: Proceedings of the Offshore Technology Conference Asia (OTC Asia), 2, pp. 1611–1621.
Stanier, S.A., Ragni, R., Bienen, B., Cassidy, M.J., 2014. Observing the effect of sustained loading on spudcans in clay. Géotechnique 64 (11), 918–926. https://doi.org/10.1680/geot.14.P.003.
Stanier, S.A., White, D.J., 2019. Enhancement of bearing capacity from consolidation: due to changing strength or failure mechanism? Géotechnique 69 (2), 166–173.
Tom, J.G., Rijnsdorp, D.P., Ragni, R., White, D.J., 2019. Fluid-structure-soil interaction of a moored wave energy device. In: Proceedings of the International Conference on Offshore Mechanics and Arctic Engineering, 58899. V010T09A024). American Society of Mechanical Engineers.
Truong, P., Lehane, B.M., Zania, V., Klinkvort, R.T., 2019. Empirical approach based on centrifuge testing for cyclic deformations of laterally loaded piles in sand. Géotechnique Vol. 69 (2), 133–145.

Verruijt, A., 1995. Computational Geomechanics. Kluwer Academic Publishers, Netherlands.
White, D.J., Doherty, J.P., Guevara, M., Watson, P.G., 2022. A cyclic py model for the whole-life response of piles in soft clay. Comput. Geotech. 141 (104519).
Zhou, Z., O'Loughlin, C.D., White, D.J., Stanier, S.A., 2020. Improvements in plate anchor capacity due to cyclic and maintained loads combined with consolidation. Géotechnique 70 (5), 448–467.